CFD INVESTIGATION OF THE EFFECT OF HEATER SPACING ON DNA AMPLIFICATION AND PRESSURE DROP IN A MICROFLUIDIC PCR DEVICE

Foteini Zagklavara[1*], Peter K. Jimack[1], Nikil Kapur[2], Osvaldo M. Querin[2], Harvey M. Thompson[2]

[1]School of Computing, University of Leeds, Woodhouse Lane, Leeds LS2 9JT,United Kingdom
[2]School of Mechanical Engineering, University of Leeds, Woodhouse Lane, LeedsLS2 9JT, United Kingdom

ABSTRACT

The development of Polymerase Chain Reaction Mullis et al. in 1986 [1] (PCR) has played an important role in the progress of molecular diagnostics, enabling the rapid DNA amplification through a series of repeated cycles. Considering the wide use of PCR devices in research, there is a great need to optimize their performance. This study focuses on the optimisation of continuous flow (CF) PCR device with serpentine-channel structure that utilises three copper wire heaters. The spacings between the heaters of the microfluidic (μ) channel are selected as the design variables, while the two objective functions of interest are the DNA amplification efficiency and total pressure drop of one PCR unitcell. Several simulations are performed using COMSOL Multiphysics 5.4®, varying the two design variables, and the values of the two objective functions are recorded. A polyharmonic spline is used to generate the response surfaces, while a genetic algorithm is used to obtain the optimum design solutions. The results indicate that there is the possibility of increasing the DNA concentration and the pressure drop by ~0.8% and ~8.6% respectively for a single PCR cycle, by modifying the distances between the three heaters.

1. INTRODUCTION

PCR requires the repetitive heating and cooling of the DNA samples in order for denaturation (~ 95 ^{o}C), annealing (~ 55 ^{o}C) and extension (~ 70 ^{o}C) to take place (Park and Park [2]). The samples need to remain in each region for the appropriate residence time (t_R) (PCR protocol). The various PCR systems developed over the years are currently used in many diagnostic systems, such as the rapid detection of infectious diseases through point-of-care (POC) diagnostics Park et al. [3], the identification of bacteria responsible for corrosion in oil and gas production systems (Zhu et al. [4], Agrawal and Lal [5]), etc..

A great number of PCR applications in microfluidic devices can be found in literature, such as the publications of Shin et al. [6], Sauer-Budge et al. [7], Yetisen and Volpatti [8] and Kim and Mi-Ree [9]. Despite the broad use of these devices, μCF-PCR devices present some limitations. The PCR mixture experiences adsorption phenomena at the flow channel interface, which leads to PCR inhibition and carryover contamination, reducing the yield of the reaction. Also, the large channel surface area to sample volume ratio enhances the adsorption of biological/chemical particles. Another drawback is the variation in the dwell times of PCR mixture (PCR mixture moves faster in the channel's centre than it does close to the surface) that results in an increase in the total residence time in the device (Zhang and Jiang, [10]).

Due to these limitations, recent research appears to also focus on the development of droplet-based μPCR devices (DR-PCR). The droplets are characterised by temperature uniformity due to their small size. These droplets act as separate chemical reactors, providing high reproducibility of reaction conditions. At the same time, the droplets provide a confined environment, preventing contamination of

*Corresponding Author: fotizagl@hotmail.com

the samples and any adsorption phenomena at the surfaces of the channel [10]. Detailed descriptions of droplet-based PCR devices can be found in the publications of Ma et al. [11], Wang et al. [12] and Shi, Xiang, and Song [13].

Despite its potential advantages, the droplet-based technology presents greater cost and complexity compared to single-phase (SP) continuous flow (CF) PCR devices [10]. Therefore, a lot of research is taking place on optimising SPCFPCR devices, in order to increase their sensitivity, specificity and their ability of multiplexing (amplifying more than one target sequence by using more than one pair of primers (Elnifro et al. [14])) (Yang and Rothman [15]).

This study presents a methodology for optimising the performance of a continuous flow (CF), single phase (SP) microfluidic (μ) PCR device, by adjusting the distance between the three copper wire heaters (corresponding to the denaturation, annealing and extension PCR temperature zones). The current design uses three heaters in order to create the required temperatures. The performance of the CFSPPCR device is simulated using COMSOL Multiphysics 5.4®, considering the design of Papadopoulos et al. [16]. Moschou et al. [17] investigated the performance of such device, where no thermal crosstalk between the three temperature zones was detected. However, even though good temperature uniformity in each zone is reported [17], the optimisation of the spacing between the heaters is investigated in the current study in order to quantify the precise effect of the heater spacing in the DNA amplification and pressure drop (objectives).

2. PROBLEM DESCRIPTION

As the fluid passes through the microchannel during a single PCR cycle (unitcell (Figure 1)), the temperature changes to ~95, ~55 and ~72 °C (denaturation, annealing and extension zones respectively) [16]. This change in the temperature of the sample aims to increase the DNA concentration by the time N ($20 < N < 35$ [16]) PCR cycles or unitcells are completed. The PCR device studied in this work consists of a series of microchannels with sigmoid-shape, and it is based on the design described by [16]. Details about the substrate materials of the chip (Kapton, PDMS and PE) and the design parameters can be found in the work of [16]. The performance of a single unitcell is simulated using COMSOL Multiphysics 5.4®, using the Laminar Flow, Conjugate Heat Transfer, Transport of Diluted Species and Joule Heating models.

2.1. Laminar Flow

Navier Stokes equations are used to describe the fluid flow in the microfluidic channel:

$$\rho(\boldsymbol{u}\cdot\nabla)\boldsymbol{u} = \nabla\cdot[-p\boldsymbol{I} + \mu(\nabla\mathbf{u} + (\nabla\mathbf{u})^T)] + \boldsymbol{F} \quad (1)$$

$$\rho\nabla\cdot\boldsymbol{u} = 0 \quad (2)$$

where ρ is the fluid density, u the velocity vector, p: the pressure, μ the viscosity and F the external forces applied to the fluid, such as gravitational force etc (McDonough [18], Gerbeau and Le Bris [19]). The Reynolds number is calculated for the case of 72°C and $Q_{vol} = 3 \cdot 10^{-11}$ m^3/s for the fluid properties of water [16] and is found equal to be ~1. As a result, the Laminar Flow model is used, while a no-slip boundary condition is implemented at the walls of the channel.

2.2. Heat Transfer

The conjugate heat transfer in steady state is presented in Equation 3:

$$\rho C_p(\boldsymbol{u}\cdot\nabla\mathrm{T}) = \nabla\cdot(k\nabla\mathrm{T}) + \sum Q_{heater,j} + \sum Q_{rad,i} + Q_{nat.conv.} \quad (3)$$

where **u** is only non-zero in the fluid domain. The $Q_{heater,j}$ is the heat generation rate of the j^{th} (j = {1, 2, 3}) heater, and is only non-zero at the j^{th} heater- Kapton interface. $Q_{rad,i}$ is the heat flux due to thermal radiation (Stefan-Boltzmann law (Equation 4)) of the i^{th} solid substrate (i = {Copper, PDMS, PE, Kapton}), and is only non-zero at the outer surfaces of the substrate materials. $Q_{nat.conv}$ is the heat flux due to the heat losses to the ambient, and is given by equation 5:

$$Q_{rad,i} = \varepsilon_i \sigma \left(T_{amb}^4 - T^4\right) \tag{4}$$

$$Q_{\text{nat.conv}} = h(T_{amb} - T) \tag{5}$$

where T_{amb}: the ambient temperature, ε_i : surface emissivity for solid i, σ: the Stefan–Boltzmann constant and h: the heat transfer coefficient.

As far as the boundary conditions are concerned: (i) a periodic temperature boundary condition is implemented at the inlet and outlets of the channel; (ii) the heater temperatures at the copper-solid interface in the denaturation, extension and annealing zones are set to T_{den} = 95 ºC, T_{ext} =72 ºC and T_{ann} = 55 ºC, respectively; (iii) periodic temperature boundary conditions are implemented at the two sides of the microchannel; (iv) a heat flux of $Q_{nat.conv}$ from equation 5 at the top, bottom, front and back sides of the microchannel, due to natural convection; (v) a heat flux of $Q_{rad,i}$ from equation 4 at the front, back, top and bottom surfaces of the unitcell. The second boundary condition is only used for the DOE simulations, providing an ideal description of the function of the heaters, in order to avoid the trial and error process required to define the electric current required for each heater. Instead, the Joule Heating model is used for the validation and mesh independence study, as performed in [16].

2.3. PCR Kinetics

The PCR kinetics and reactions are presented in detail in [16] and are introduced in COMSOL Multiphysics 5.4®(Transport of Diluted Species Model). Equation 6 provides the general form of the mass conservation of species in steady state:

$$\nabla \cdot J_k + \boldsymbol{u} \cdot \nabla C_k = R_k \tag{6}$$

$$J_k = -D_k \nabla C_k \tag{7}$$

where C_k is the concentration of the k^{th} species (k={1,2,..,7} corresponding to S_1S_2, S_1, S_2, P_1, P_2, S_1P_2 and P_1S_2 respectively): R_k is the reaction rate of the k^{th} species and D_k: the diffusion coefficient of the k^{th} species. As far as the boundary conditions are concerned, a zero-flux boundary condition is implemented at the walls of the microfluidic channel. The inlet concentrations of the seven species can be found at [18], together with the diffusion coefficients, D_k, of Equations 6.

3. METHODOLOGY

3.1 Validation of the model

The model of the μPCR unitcell presented in Sections 2.1-2.3 is implemented in COMSOL Multiphysics 5.4® and is validated with the work of [16]. For the validation and the mesh independence study, the Joule Heating model is used to describe the function of the copper wire heaters.

Five different meshes (~164,000, ~321,000, ~ 866,000, ~ 4,036,000, ~6,133,000 elements) are tested as part of a mesh independence study, in order ensure that the results of the simulations both converge and are independent of the mesh resolution. As a result of this study, the ~321,000 elements mesh is selected, since the solution generated by this mesh is mesh independent (the values of $log_2 \frac{[DNA]}{[DNA]_o}$, ΔP and Ph are compared to the reference values [16]).

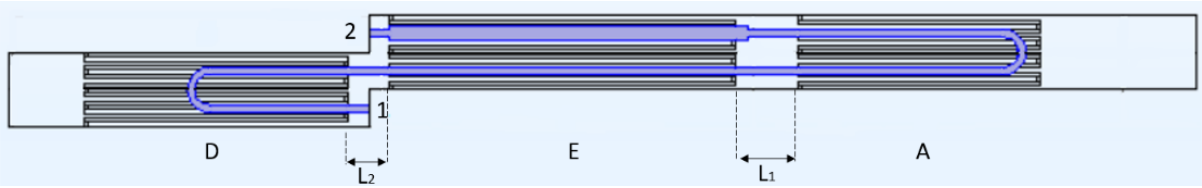

Figure 1: Schematic graph of a unitcell. Points 1, 2, D, E and A present the entrance, exit, denaturation, extension and annealing zones of the unitcell respectively. A copper wire heater is located in each of the three temperature regions.

3.2 Optimisation Method

After the completion of the mesh independence study and the validation of the current model with the one presented in [16], the optimisation problem is formulated. The spacings between the three copper wire heaters, L_1,L_2 (Figure 1), are selected as the two design variables, with lower and upper limits of 500 and 2500 μm respectively (design domain). The pressure drop and the DNA amplification (DNA amplification is expressed as $log_2 \frac{[DNA]}{[DNA]_o}$, where [DNA] is the DNA concentration at the end of the channel (Point 2, Figure 1) and $[DNA]_o$ the initial DNA concentration (Point 1, Figure 1)) are selected as the two objective functions of interest.

After formulating the optimisation problem, the response surfaces of the two objective functions are generated. This is accomplished by developing the metamodels of the two objective functions using Design of Experiments (DOE) and COMSOL Multiphysics 5.4®. More specifically, 80 DOE points are generated using Morris Mitchel Latin Hypercubes (Julie, [20]), while COMSOL Multiphysics 5.4® is used to simulate the performance of the unitcell (fluid flow, heat transfer and PCR kinetics). The response surfaces are generated using a third order polyharmonic spline (Wiens, [21]), while the optimum design solutions are located using the genetic algorithm (MathWorks, [22]).

4. RESULTS

The response surfaces of $-log_2 \frac{[DNA]}{[DNA]_o}$ and ΔP are presented in Figure 2. The values presented are dimensionless and scaled between 0-1. After locating the optimum design solutions, the Joule Heating model is used to obtain the values of the two objective functions considering a more realistic function of the copper wire heaters. The results indicate that there is the possibility of improving the two objective functions ($log_2 \frac{[DNA]}{[DNA]_o}$ and pressure drop) for a PCR cycle by ~1.8% (for Design 1: [L_1,L_2] = [2500 μm, 2500 μm]) and ~8.6% (for Design 2: [L_1,L_2] = [500 μm, 500 μm]) respectively, by modifying the distances between the three heaters. The values of the pressure drop and the DNA amplification are presented in Table 1.

Table 1: Results of the optimisation problem

Design Cases	L_1 (μm)	L_2 (μm)	$log_2 [DNA]/[DNA]_o$ (-)	Δp (Pa)
Design 1	2500	2500	0.678*	319.63*
Design 2	500	500	0.646*	259.86*
Design of [16]	1670	1110	0.666*	284.29*

* Values obtained using the Joule Heating Model

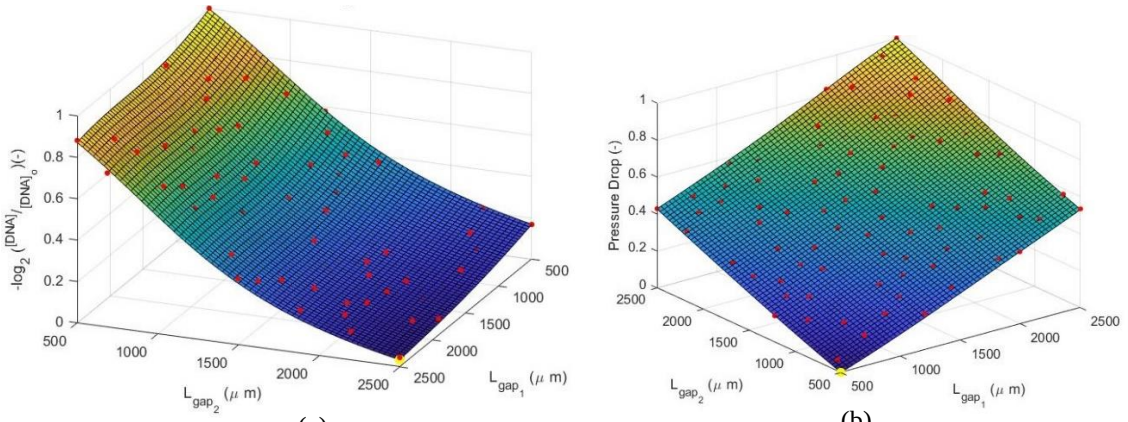

(a) (b)

Figure 2: Response surfaces generated with polyharmonic function [21] for (a) $-log_2 \frac{[DNA]}{[DNA]_o}$ and (b) pressure drop. The green points present the optimum solutions for the $-log_2 \frac{[DNA]}{[DNA]_o}$ and pressure drop respectively, generated with genetic algorithm [22].

5. CONCLUSION

Considering the results presented in this work, increasing the spacing between the heaters appears to lead to an improvement to the DNA amplification of a unitcell, while minimising the spacing reduces the pressure drop. Further work is expected to focus on examining the effect of other design variables on the DNA amplification and pressure drop.

ACKNOWLEDGEMENTS

The funding was received by EPSRC [23].

REFERENCES

[1] Kary Mullis et al. “Specific enzymatic amplification of DNA in vitro: the polymerase chain reaction”. In: Cold Spring Harbor symposia on quantitative biology. Vol. 51. Cold Spring Harbor Laboratory Press. 1986, pp. 263–273.

[2] Jaehyun Park and Heesung Park. “Thermal cycling characteristics of a 3D-printed serpentine microchannel for DNA amplification by polymerase chain reaction”. In: Sensors and Actuators A: Physical 268 (2017), pp. 183–187.

[3] Seungkyung Park et al. “Advances in microfluidic PCR for point-of-care infectious disease diagnostics”. In: Biotechnology advances 29.6 (2011), pp. 830–839.

[4] XY Zhu et al. “Rapid detection and quantification of microbes related to microbiologically influenced corrosion using quantitative polymerase chain reaction”. In: Corrosion 62.11 (2006), pp. 950–955.

[5] Akhil Agrawal and Banwari Lal. “Rapid detection and quantification of bisulfite reductase genes in oil field samples using real-time PCR”. In: FEMS microbiology ecology 69.2 (2009), pp. 301–312.

[6] Young Shik Shin et al. “PDMS-based micro PCR chip with parylene coating”. In: Journal of Micromechanics and Microengineering 13.5 (2003), p. 768.

[7] Alexis F Sauer-Budge et al. “Low cost and manufacturable complete microTAS for detecting bacteria”. In: Lab on a Chip 9.19 (2009), pp. 2803–2810.

[8] Ali K Yetisen and Lisa R Volpatti. “Patent protection and licensing in microfluidics”. In: Lab on a Chip 14.13 (2014), pp. 2217–2225.
[9] Sung Woo Kim and KIM Mi-Ree. High-speed real-time PCR device based on lab-on-a-chip for detecting food-borne bacteria to agrifood, and methods for detecting food-borne bacteria to agrifood using the same. US Patent 10,245,590. Apr. 2019.
[10] Yonghao Zhang and Hui-Rong Jiang. “A review on continuous-flow microfluidic PCR in droplets: Advances, challenges and future”. In: Analytica chimica acta 914 (2016), pp. 7–16.
[11] Shou-Yu Ma et al. “Peanut detection using droplet microfluidic polymerase chain reaction device”. In: Journal of Sensors 2019 (2019).
[12] Wei Wang et al. “Droplet-based micro oscillating-flow PCR chip”. In: Journal of Micromechanics and Microengineering 15.8 (2005), p. 1369.
[13] Jian Shi, Shuanghong Xiang, and Xiaohui Song. Droplet digital pcr chip. US Patent App. 16/465,438. Jan. 2020.
[14] Elfath M Elnifro et al. “Multiplex PCR: optimization and application in diagnostic virology”. In: Clinical microbiology reviews 13.4 (2000), pp. 559–570.
[15] Samuel Yang and Richard E Rothman. “PCR-based diagnostics for infectious diseases: uses, limitations, and future applications in acute-care settings”. In: The Lancet infectious diseases 4.6 (2004), pp. 337– 348.
[16] Vasileios E Papadopoulos et al. “Comparison of continuous-flow and static-chamber μPCR devices through a computational study: the potential of flexible polymeric substrates”. In: Microfluidics and Nanofluidics 19.4 (2015), pp. 867–882.
[17] Despina Moschou et al. “All-plastic, low-power, disposable, continuous-flow PCR chip with integrated microheaters for rapid DNA amplification”. In: Sensors and Actuators B: Chemical 199 (2014), pp. 470– 478.
[18] JM McDonough. “Lectures in elementary fluid dynamics”. In: University of Kentucky, Lexington, KY (2009), pp. 40506–0503.
[19] J-F Gerbeau and Claude Le Bris. “A basic remark on some Navier-Stokes equations with body forces”. In: Applied Mathematics Letters 13.3 (2000), pp. 107–112.
[20] Julie. Surrogate Model Optimization Toolbox, MATLAB Central File Exchange. 2012. url: https: //www.mathworks.com%20/matlabcentral/fileexchange/%2038530-surrogate-model%20-optimization-toolbox. (accessed: 14.05.2020).
[21] Travis Wiens. Radial Basis Function Network. 2014. url: https ://www.mathworks.com/% 20matlabcentral/%20fileexchange/%2022173-radial-basis-function-network. (accessed: 14.05.2020).
[22] MathWorks. Genetic Algorithm. 2021. url: https : //uk.mathworks.com/help/gads/ga.html. (accessed: 06.01.2021).
[23] EPSRC. EPSRC Centre for Doctoral Training in Fluid Dynamics at Leeds. 2021. url: https://gow. epsrc.ukri.org/NGBOViewGrant.aspx?GrantRef=EP/L01615X/1. (accessed: 25.02.2021).